A 3D numerical model to investigate mechanical, thermal and material flow characteristics in friction stir welding of copper sheets

H. Pashazadeh[1], A. Masoumi[2], J.Teimournezhad[3]

1Ph.D Student, 2 Associate Professor, 3Assistant Professor, School of Mechanical Engineering, College of Engineering, University of Tehran

hamed_pashazadeh@yahoo.com

Abstract

The objective of this study was to develop a numerical model for the prediction of temperature distribution, effective plastic strain distribution, and especially material flow in friction stir welding of copper plates. The DEFORM-3D software was used by incorporating a lagrangian incremental formulation. Three-dimensional results of the material flow pattern which were extracted using the point tracking are in good agreement with the experiment. It was shown that the main part of material flow occurs near the top surface. Material near the top surface at the behind of tool stretches from retreating side towards advancing side which leads to non-symmetrical shape of the stir zone. The stir zone shape in FSW of copper alloys, which was predicted by simulation, does not lean completely towards any sides of welding line.

Keywords: *Finite element modeling, Friction stir welding, Material flow, Temperature distributions, Strain distributions*

1. Introduction

The automotive industry, featuring large manufacturing batches, six sigma requirements and challenging material combinations, from wrought and cast aluminum to magnesium and copper alloys, provides a perfect field for FSW applications. Friction stir welding (FSW) can be an important joining technology for the automotive industry. In fact, this welding process is probably the solution to overcome some of the usual problems associated with the fusion welding of aluminum alloys, but is also an important step in nowadays environmental concerns by the possibility of reducing material waste and avoiding radiation and harmful gas emissions usually associated with the fusion welding processes. In principle, all aluminum components in a car can be friction stir welded: bumper beams, rear spoilers, crash boxes, alloy wheels, air suspension systems, rear axles, drive shafts, intake manifolds, stiffening frames, water coolers, engine blocks, cylinder heads, dashboards, roll-over beams, pistons, etc. Minor modifications to the structure may be needed in order to make it more suitable for FSW, but these should not be insurmountable.

To-date, the interest and application of FSW in the automotive industry has been in three general categories. These three categories include the joining of extrusions to form "larger extrusions," joining of tailor welded blanks, and joining for various assembly applications. FSW in each of these categories has distinct benefits and resulting cost reductions and/or other advantages that allow its application to be beneficial. Each of these categories will be discussed in more detail. For each of these categories, joint design is an important consideration. For the joining of extrusions and general assembly applications, there are two basic joint configurations that will likely be employed. These two joint designs are the partial penetration butt weld and the lap weld, as these are the most capable of handling process variations inherent in high volume production. However, the tailor welded blank requires a full penetration butt weld, but production variations are less significant in this application, allowing FSW of tailor welded blanks to be feasible. In all of these applications, the travel speeds of FSW originally would have been too slow to economically justify the use of FSW. However, through extensive process development efforts the travel speeds have improved, and as such, is not an issue anymore.

Demand for materials with high strength, thermal and electrical conductivity, and wear resistance has been increased in recent years and among them,

copper alloys which are mainly used for electronic and thermal products such as electrical contacts, electronic packaging and resistance welding electrodes have been attracted researchers for investigation their behaviour in Friction Stir Welding (FSW). Although, welding of aluminum alloys have been reported in numerous studies, but few studies have been conducted in the FSW of copper and its alloys. High melting point and good thermal conductivity which require higher heat input are the main reasons of such restriction. Andersson and Andrews [1] investigated Friction Stir Welding of copper to copper. Their experiment showed that the threaded pin is suitable for welding of copper plates with a thickness of 3 mm, but it is not suitable for welding of 10 mm thick plates because the threads of tool are filled by copper. Their experiments also showed that the sintered tungsten-based alloy pin is suitable for thick plates welding. Hautala and Tiainen [2] experiments showed that tools which made from superalloy and hot working tool steel create a weld with good quality whereas sintered tungsten carbide is brittle for FSW of copper. Xue et al. [3] achieved sound joints of pure copper under low heat input conditions (rotational speeds of 400-800 rpm and traverse speed of 50 mm/min) with threaded tool. Their experimental results revealed that grain size reduced from 9 to 3.5 μm by reducing the rotational speed from 800 to 400 rpm. Cederqvist et al. [4] studied the reliability of friction stir welded copper canisters containing Sweden's nuclear waste. They investigated different rotational and traveling speed and shoulder depth. The shoulder and pin material in their study were sintered tungsten alloy Densimet and nickel-based superalloy Nimonic 105, respectively and the tool pin geometry was threaded.

Among the studies about FSW of copper, the effect of FSW parameters on weld quality have been investigated experimentally, but process simulation has not been reported, widely. Simulation of processes enables users to forecast properties changes during the process. Advantage of simulation-based approaches is their predictability over experimental ones. Therefore, the effect of various parameters on the mechanical and thermal properties and their interaction on each other could be investigated before doing any experimental test. Some researchers made efforts to develop numerical codes for FSW process. In spite of the simple concept of FSW, details of the process such as heat generation and material flow are complex. Understanding the temperature distributions in the workpiece during FSW is an essential subject due to its effects on the grain size and thermal residual stresses and subsequently, the strength.

FSW process simulations can be done by three different methods: (i) Arbitrary Lagrangian-Eulerian (ALE) formulation; (ii) Lagrangian incremental formulation; and (iii) Eulerian method. The first and second method is based on solid mechanics and third approach is based on fluid dynamics.

Guerdoux and Fourment [5] developed FSW modelling based on ALE formulation which utilizing 3D Forge3 finite element software with automatic remeshing to predict the temperature and plastic strain distribution and material flow during FSW of an aluminium alloy. They used the experimental data of temperature and force to calibrate their model. Reported researches of Xu et al. [6], Fourment et al. [7], Buffa et al. [8], Schmidt and Hattel [9-10] and Zhang et al. [11] also have been conducted by the ALE method. On the other hand, Bendzsak et al. [12], Shercliff and Colegrove [13], Ulysse [14], Seidel et al. [17], Colegrove et al. [16-20], Nandan et al. [21] , Bastier et al. [22-23], and Kim et al. [24] used Eulerian method to develop their model. Different friction conditions could be considered in Eulerian models and reported works show that either sticking [12, 15 and 19] or sticking/sliding conditions [21 and 22] have been used. Bastier et al. [22] conducted an Eulerian based FSW simulation and reported results showed that material velocity near the tool pin is about 1% of the FSW tool velocity.

Buffa et al. [8 and 25], Asadi et al. [26] and Tutunchilar et al. [27] used Lagrangian incremental formulation to simulate FSW process. In the proposed model by Asadi et al. [26], material flow was predicted using the point tracking and results showed that material on the advancing side experiences more plastic strain than that of the retreating side material.

Most of the reported experimental and numerical researches concerns investigation on FSW of aluminum alloys, while studies of copper welding are a few and so far no simulation was performed for FSW of copper. Therefore, the aim of this work is to investigate copper friction stir welding through simulation approach. To achieve this goal, a 3D lagrangian incremental finite element simulation was developed to predict temperature, effective plastic strain, and especially material flow in the stir zone. Three-dimensional results of the material flow pattern were extracted using the point tracking option. The stir zone shape which was predicted by simulation is in good agreement with the experimental result.

2. Numerical Model Details

Deform-3D software was used to simulate the FSW process with the Arbitrary Lagrangian Eulerian (ALE) formulation. Also, it was assumed that: (1) the

workpiece is modeled as a rigid-viscoplastic material; (2) the tool is rigid; (3) the friction factor between the work piece and the tool is constant; and (4) the thermal characteristics of the work piece and tool are constant. All of the free surfaces of the work piece and the tool were surrounded by the atmosphere at the ambient temperature. The work piece was fixed in the bottom surface from all directions. Furthermore, simulation was done based on following assumptions and conditions:

3. Governing Equations

The rigid-viscoplastic FEM is implemented widely in the simulation of metal forming. The traditional rigid-viscoplastic FEM is derived from a variational principle, which results in nonlinear equations. These equations can be solved by iterative methods (such as the commonly used Newton-Raphson method). The following equations present the basic governing equations for rigid-viscoplastic metal [28]:

$$\sigma'_{ij} = (\frac{2\bar{\sigma}}{3\dot{\bar{\varepsilon}}})\dot{\varepsilon}_{ij} \tag{1}$$

It is assumed that the material follows the Von Misses yield criterion and the associated flow rule is:

$$\bar{\sigma} = \sqrt{\frac{3}{2}}\left\{\sigma'_{ij}\sigma'_{ij}\right\}^{1/2} \tag{2}$$

$$\dot{\bar{\varepsilon}} = \sqrt{\frac{3}{2}}\left\{\dot{\varepsilon}_{ij}\dot{\varepsilon}_{ij}\right\}^{1/2} \tag{3}$$

Where $\bar{\sigma}$, $\dot{\bar{\varepsilon}}$, σ'_{ij} , and $\dot{\varepsilon}_{ij}$ are the effective stress, effective strain rate, deviator stress components and strain rate components, respectively. The effective stress $\bar{\sigma}$ is a function of effective strain, effective strain rate and temperature as follow:

$$\bar{\sigma} = \bar{\sigma}(\bar{\varepsilon}, \dot{\bar{\varepsilon}}, T) \tag{4}$$

The variation method is based on variation principles. It requires acceptable velocities u_i that satisfy the conditions of compatibility and incompressibility and the velocity boundary conditions. The actual solution gives the following functional a stationary value:

$$\pi = \int_V E(\dot{\varepsilon}_{ij})dV - \int_{S_F} F_i u_i ds \tag{5}$$

Where F_i is surface tractions, u_i the velocity components, V the volume of the work piece, S_F the force surface, and $E(\dot{\varepsilon}_{ij})$ the work function, which gives.

$$\sigma'_{ij} = \frac{\partial E}{\partial \dot{\varepsilon}_{ij}} \tag{6}$$

The solution of the original boundary-value problem is then obtained from the solution of the dual variational problem, where the first-order variation of the functional vanishes, namely,

$$\delta\pi = \int_V \bar{\sigma}\delta\dot{\bar{\varepsilon}}dV - \int_{S_F} \delta u_i ds = 0 \tag{7}$$

To remove the constraint, the penalized form is used for the incompressibility as:

$$\delta\pi = \int_V \bar{\sigma}\delta\dot{\bar{\varepsilon}}dV + \int_V K\dot{\varepsilon}_V\delta\dot{\varepsilon}_V dV - \int_{S_F} F_i\delta u_i ds = 0 \tag{8}$$

Where penalty constant K is a large positive constant for volume change, and $\dot{\varepsilon}_V = \dot{\varepsilon}_{ii}$ is the volumetric strain rate. In Eq. (8), δu_i is arbitrary variation and $\delta\dot{\bar{\varepsilon}}$ and $\delta\dot{\varepsilon}_V$ are the variations of strain rate derived from δu_i. Eq. (8) is the basic equation for the Lagrangian finite element formulation.

This rigid-viscoplastic material model is coupled with a heat transfer model, expressed by the following equation [29]:

$$(KT_{,i})_{,i} + \dot{r} - (\rho c_p T) = 0 \tag{9}$$

Where K denotes thermal conductivity, $\dot{r}$ the heat generation rate, T the temperature, and ρ the specific density and c_p the specific heat. The first term $(KT_{,i})_{,i}$ and the third term $\rho c_p T$ represent the heat transfer rate and the internal heat energy generation rate, respectively. The rate of the heat generation in the workpiece due to the plastic deformation is given below:

$$\dot{r} = k\rho\varepsilon \tag{10}$$

k represents the fraction of mechanical energy converted to heat and is assumed to be 0.9. The fraction of the remainder of the plastic deformation energy is associated with causing changes in dislocation density, (sub-) grain boundary generation

and migration, and phase transformation and evolution. Along the boundary of the workpiece, either the temperature T is prescribed or a heat flux

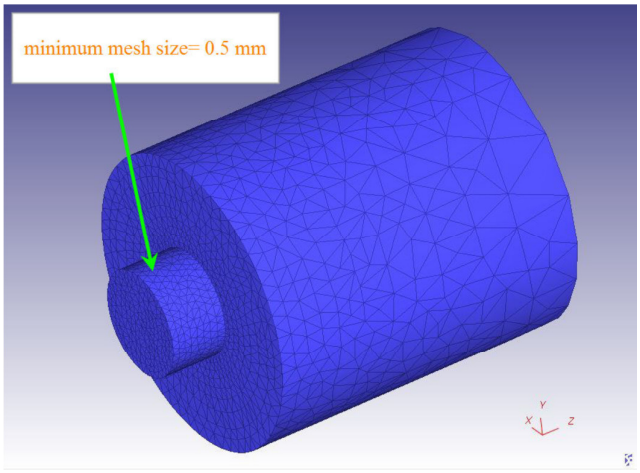

Fig1. Schematic illustration of tool.

is given. The energy balance equation can be written using the weighted residual method as:

$$\int_V KT_{,i}\delta T_{,i}dV+\int_V \rho c_p \dot{T}dT-\int_V k\sigma_{ij}\varepsilon_{ij}\delta TdV-\int_{S_q} q_n\delta Tds=0 \quad (11)$$

In which, q_n is the heat flux normal to the boundary surface. In general, q includes the convection heat loss and the radiation heat loss to the environment, and the frictional heat gain due to the relative movement between the tool and work piece. The temperature distribution of both the work piece and the tool can be obtained readily by solving energy equilibrium equation above.

4. Friction Model

Constant shear friction is used mostly for bulk-forming simulations. The frictional force in the constant shear model is defined by:

$$f = mk \quad (12)$$

Where f is the frictional stress, k the shear yield stress, and m the friction factor. Thus, the friction is a function of the yield stress of the deforming body. Friction factor of 0.45 was chosen [21].

5. Work Piece and Tool Models

The tool was considered to be rigid and was meshed with minimum mesh size of 0.5 mm. As shown in Figure 1, the smallest elements were placed in the tool pin and away from the pin mesh size becomes larger. The work piece was modeled as a rigid viscoplastic material and was meshed with ~42,000 tetrahedral elements. To prevent element distortion, automatic local re meshing was taken into account for the work piece elements.

6. Material Properties, Boundary Conditions and Welding Parameters

The work piece material model was assumed to be rigid-viscoplastic. In the other words; the elastic region of material was disregarded. Flow stresses of the pure copper at different strain rates and temperatures were interpolated in logarithmic space of strain and strain rate and linear space of temperature [30]. The relationship between flow stress and strain for material at temperature 500, 800, and 900 °C, and strain rates of 0.001-100 s-1 are shown in Figure 2. In this study, FSW tool and back plate were modeled as rigid. Thermal properties of the work piece, FSW tool, and back plate were considered constant and their values are given in Table 1. Heat exchange between ambient air (with temperature of 20 °C) and free surfaces of the work piece and tool were taken into account (see Table 1). Simulation parameters (welding parameters such as rotational and traverse speeds tilt angle and plunge depth of shoulder) are given in Table 2.

7. Results and discussion

7.1 Temperature distribution

In this section, temperature result of FSW process from FEM model has been compared with the experimental result of Hwang et al. [31]. To maintain consistency, the dimensions of the workpiece, material properties, welding conditions and boundary conditions used were the same as Hwang et al. [31]. A comparison between measured temperature data of weld nugget from Hwang and the calculated results from FEM simulation at a tool rotational speed of 900 rpm and a traverse speed of 50 mm/min is shown in Fig. 3. This thermal history was captured for the point with 6 mm distance from welding line. It indicates a good agreement between the calculated results and measured data.

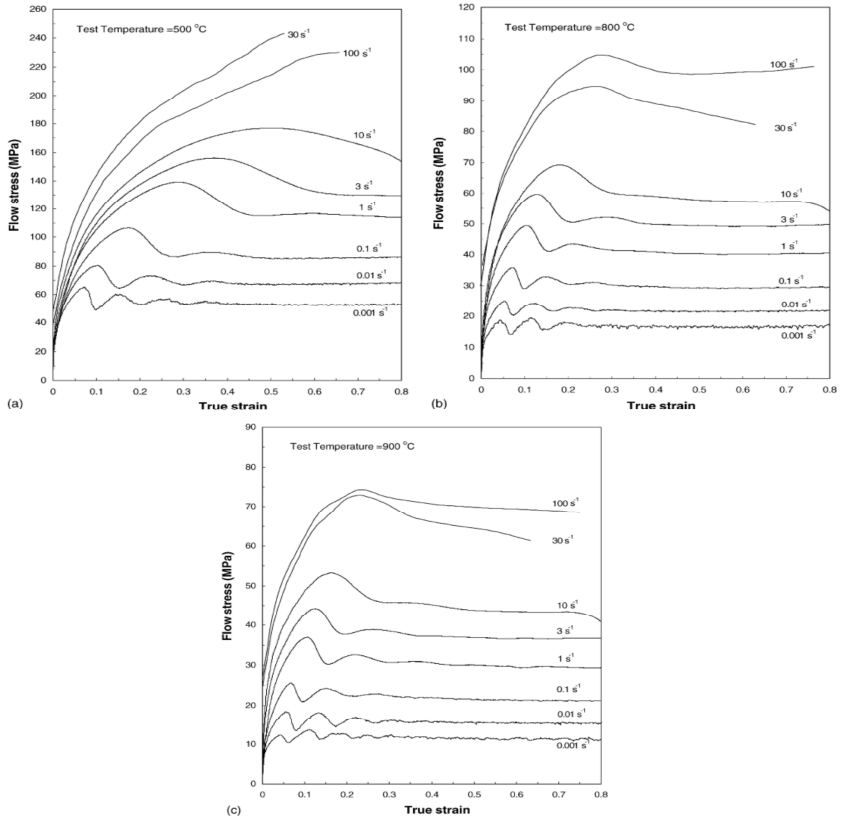

Fig2. Flow stress-strain curves of base metal under different conditions [30]

Table 1: Thermal characteristics of work piece, tool, backing plate

Property	Cu	FSW Tool (H13)	Back-plate
Heat capacity ($N/mm^2.^\circ C$)	4.42	3.24	-
Emissivity	0.64	0.7	-
Conductivity ($N/s.^\circ C$)	371	24.5	-
Heat transfer coefficient between tool and billet ($N/mm.s.^\circ C$)	11	11	-
Heat transfer coefficient between backing plate and billet ($N/mm.s.^\circ C$)	1	-	1
Heat transfer coefficient between tool/work piece and air ($N/mm.s.^\circ C$)	0.02	0.02	-

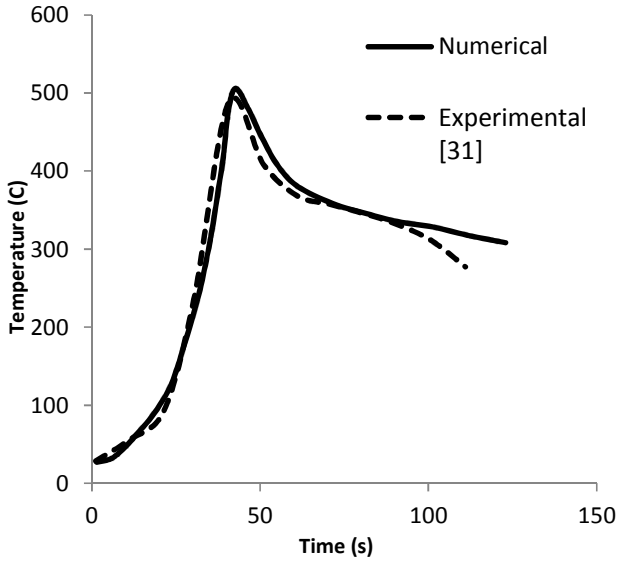

Fig3. Temperature history derived from simulation and experiment [31] at 6 mm from the welding line

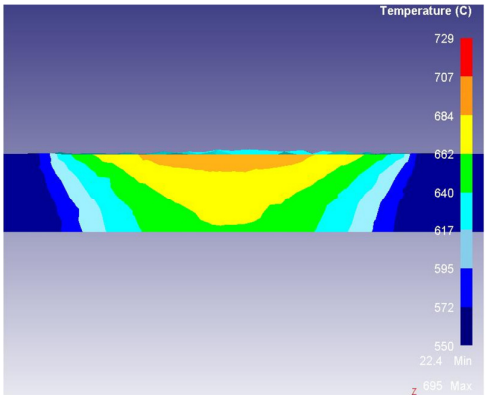

(a) v=40mm/min,w=630rpm

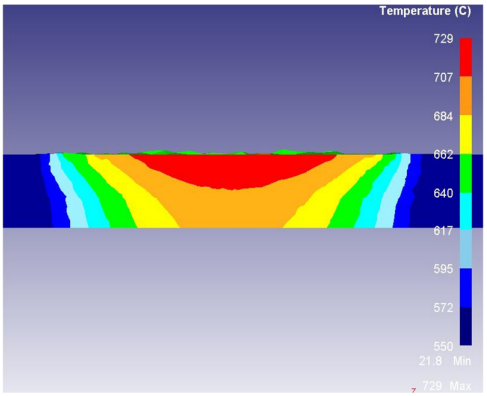

(b) v=40mm/min,w=710rpm

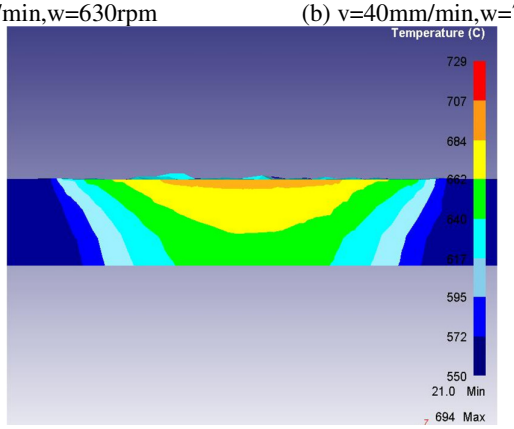

(c) v=63mm/min,w=710rpm

Fig4. Temperature distribution at different welding parameters

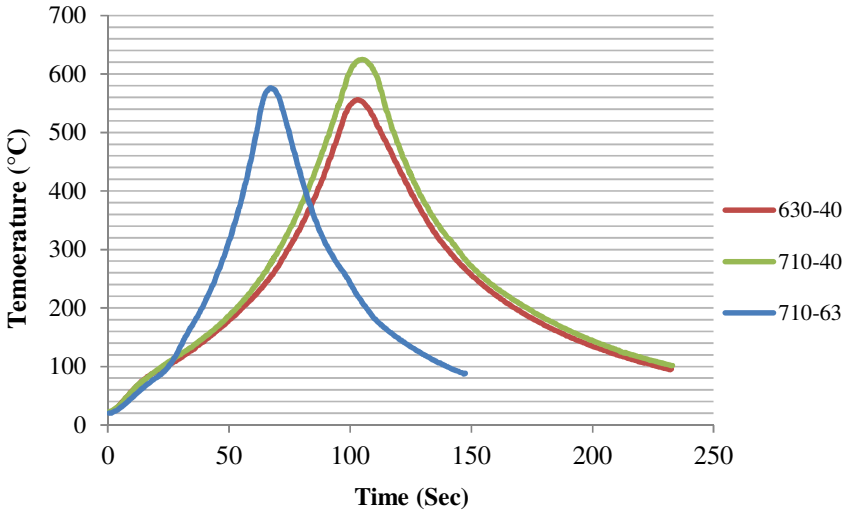

Fig5. Thermal history of HAZ at different welding parameters

The temperature contours along the transverse direction under different welding conditions are shown in Figure 4. These contours are presented at the transverse direction after 20 mm tool translation, and time zero corresponds to the start of the tool translation. As shown in Figure 4, maximum temperature in weld No. 1, No. 2 and No. 3 are 652, 724 and 682 °C, respectively. The temperature distribution is asymmetric around the tool pin and maximum temperature is found at the work piece/shoulder interface and behind of the pin. On the other hand, the temperature of the advancing side (AS) was slightly higher than that of the retreating side (RS) because plastic deformation is more severe at the AS. This observation is consistent with other studies [11]. The temperature distribution investigation does not provide a clear understanding of the process. For a better understanding of the process it is also necessary to determine the temperature history of welds. Fig. 5 represents the thermal history of HAZ for translational stage. These measurements were provided for a point that was located 2 mm below the work piece surface and at a distance of 9 mm from the joint line on the advancing side. In the constant traverse speed of 40 mm/min, increasing the rotational speed from 630 (weld No.1) to 710 (weld No.2) rpm does not cause significant changes in thermal history. However, the maximum temperature in the weld No. 2 is 69°C higher than that of the weld No. 1. Nevertheless in the constant rotational speed of 710 rpm, increasing the traverse speed from 40 (weld No.2) to 63 mm/min (weld No.3) leads to a considerable variation in the thermal history. During FSW, the thermal cycle results annealing softening in the HAZ, because various dislocation structures disappeared in the recovery and/or recrystallization processes. There is no doubt that the softening degree of the HAZ was affected by the peak temperature and the duration at high temperatures. For the weld No. 1, 2 and 3, the time which they were exposed on temperature above 200 °C, were 112, 119 and 67 second respectively. It is clear that the

Cooling rate in weld No.3 is higher than weld No.1 and 2. Besides, higher traverse speeds will reduce the welding time. Subsequently, the work piece will stay less time at high temperatures. As observed, the thermal history provides a better understanding of the process.

8. .Effective Plastic Strain and Strain Rate

It is obvious that the microstructure of the weld nugget is influenced by thermal cycle and plastic deformation due to the mechanism of dynamic recrystallization. In fact, the grain size will be decreased with the increase of the plastic strain and strain rate and decreasing of the temperature.

Fig. 6 shows the effective plastic strain distribution in the transverse section of welds. For better understanding, the measurements also were carried out along a line 2 mm under the shoulder and the behind of pin after 20 mm tool translation which is shown in Figure 7. In Fig. 7 the negative values on the horizontal axis correspond with the retreating

side. As seen in Figures 6 and 7, effective plastic strain distribution in the transverse section is asymmetric and the maximum of the effective plastic strain occurs on the advancing side and near the top surface due to different material flow patterns, and also frictional forces of the shoulder.

As can be seen from the Figures 6 and 7, around the pin, the value of the equivalent plastic strain distribution is greater and the maximum value does not occur in welding line, rather on the advancing side near the welding line. This shows that the material flow on the advancing side and on the retreating side are different, which causes that the deformation of material near the welding line is not symmetric.

By increasing the rotational speed from 640 to 710 rpm, the imposed plastic strain and the width of the deformed material along the transverse direction is increased. As can be seen in Figure 7, increasing the traverse speed from 40 to 63 mm/min leads to reduction in imposed strain and the width of the deformed material. Another point in Figures 6 and 7 that requires further explain, is the reduction of strain gradient in the traverse section by reducing the tool rotational speed and increasing the tool traverse speed. Zhang et al. [11] concluded the increasing strain gradient is a reason for reduction of the material mixture. This shows that the suitable selection of the rotational and traverse speed is very important in FSW.

Fig. 8 shows the welds strain rate history. The point tracking option of software was used to extract these results. Effective strain rate in FSW was computed by Schmidt and Hattel [9 and10], Zhang et al. [11], Kim et al. [24], and Buffa et al. [8 and 25]. The reported maximum values of strain rate varied from 4 to 3000, for various welding conditions. As can be seen in Figure 8, increasing the tool rotational and traverse speed lead to an increase in the strain rate.

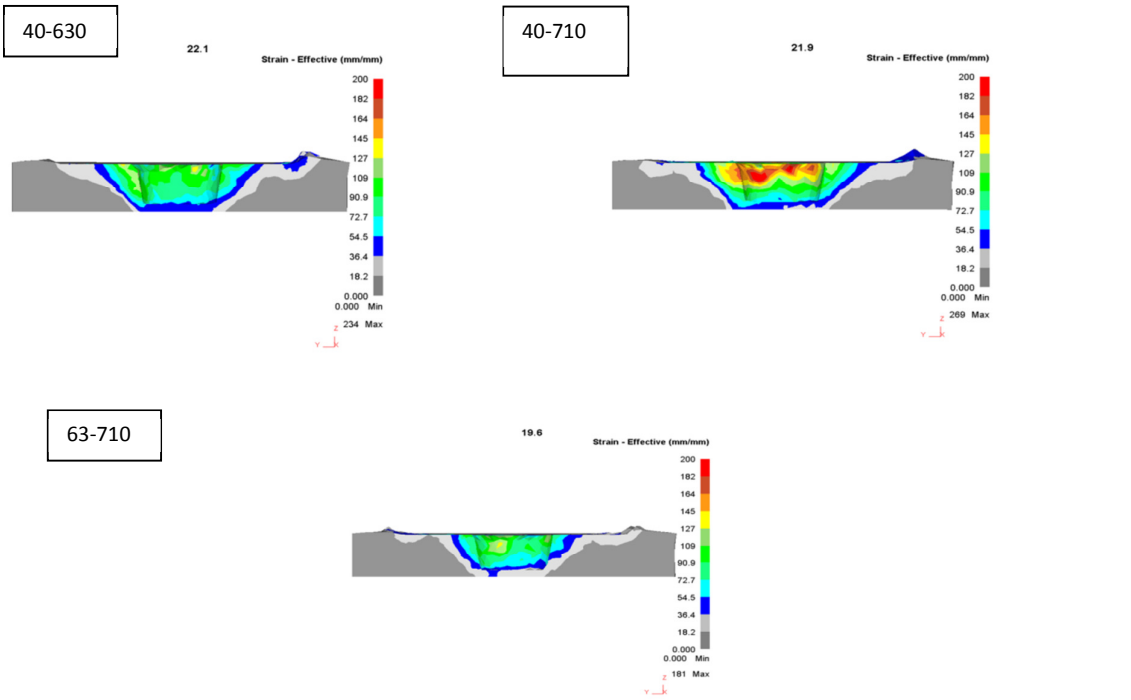

Fig6. Effective plastic strain distribution for different welding parameters

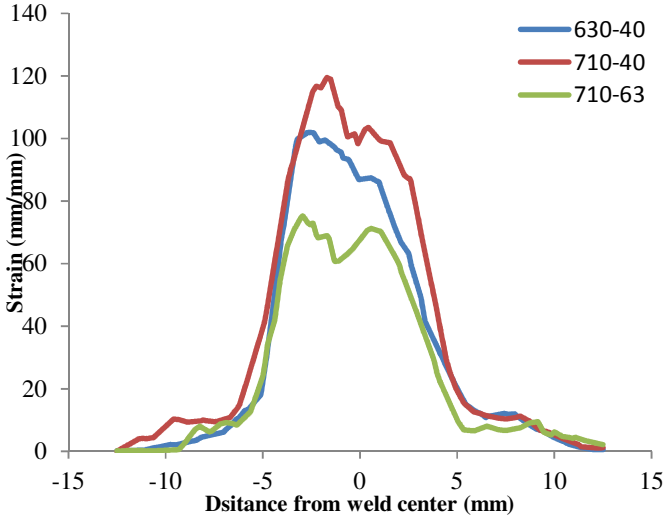

Fig7. Effective plastic strain variation versus distance from welding line

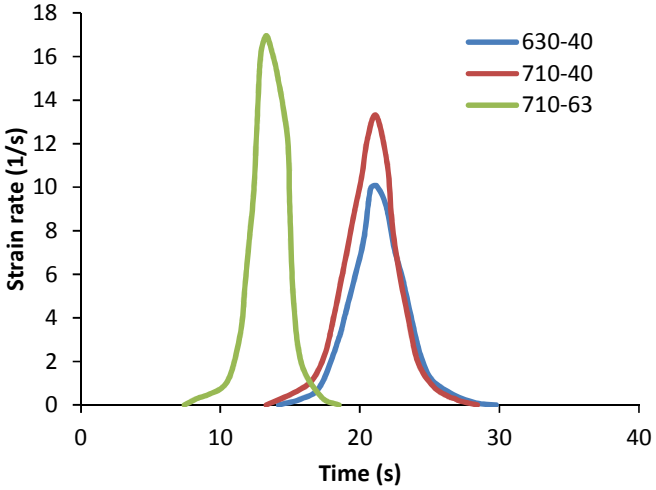

Fig8. The welds strain rate history

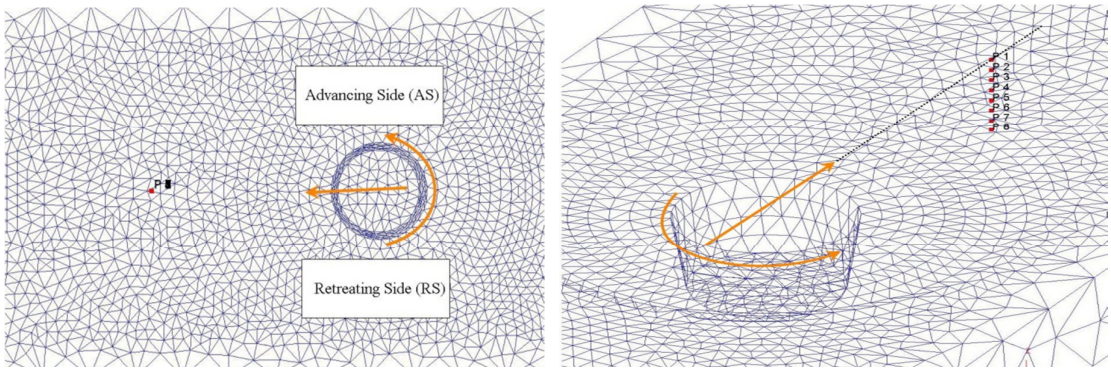

Fig9. Initial positions of particles on the welding line that has been selected for material flow patter

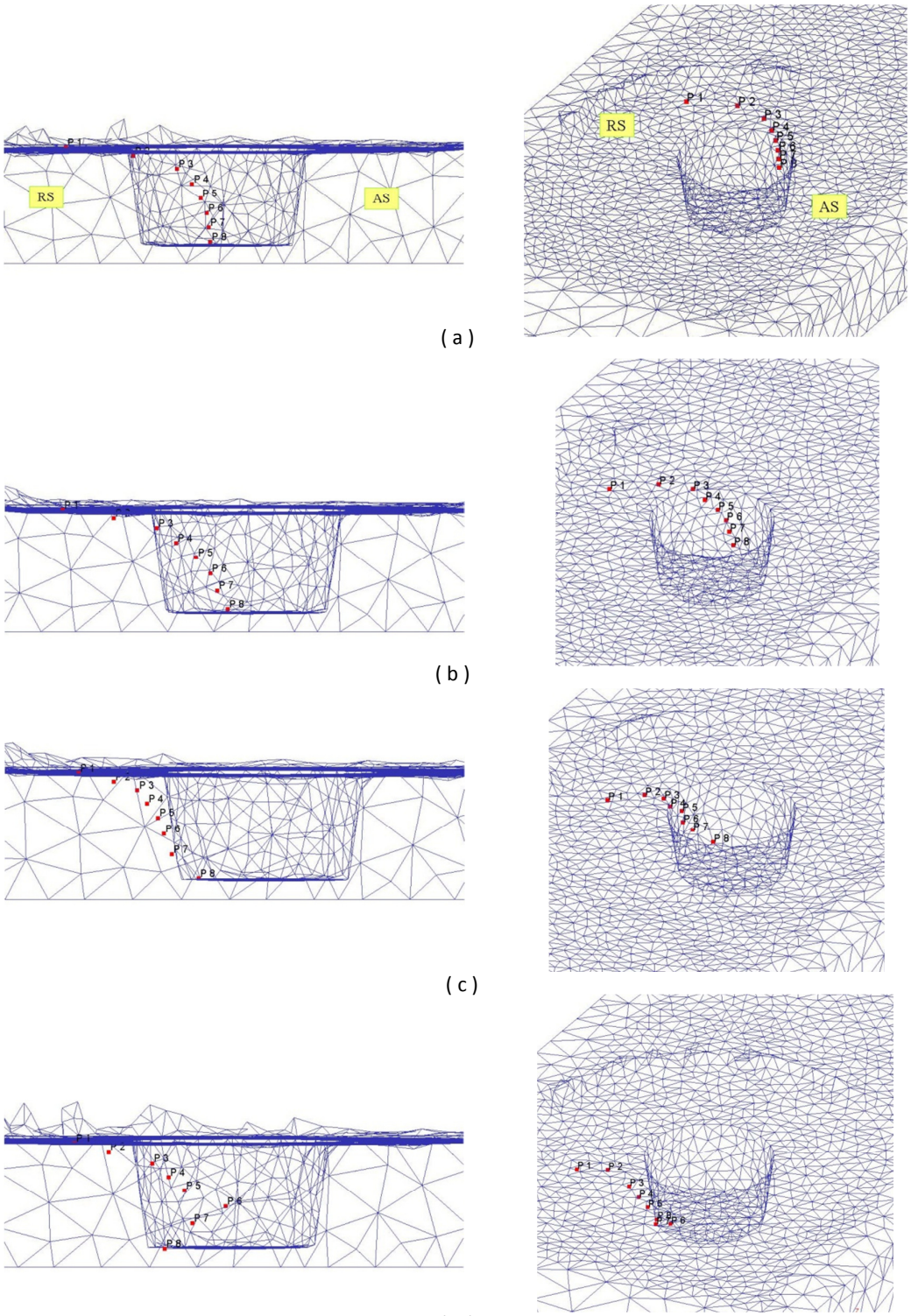

Fig10. Material flow pattern on the center line

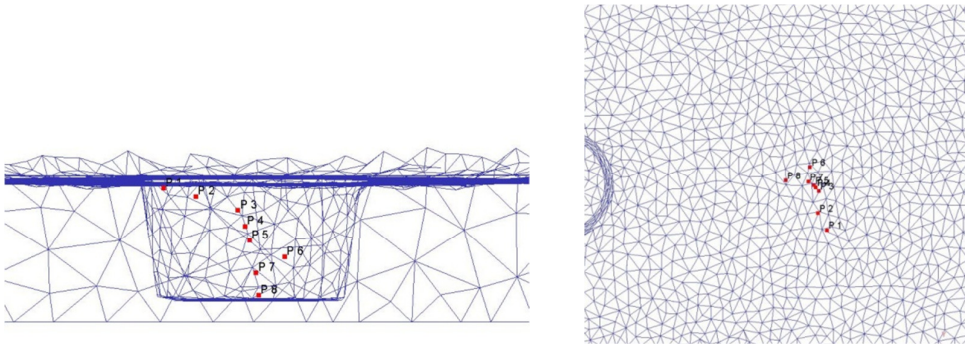

Fig11. Final positions of centre line points

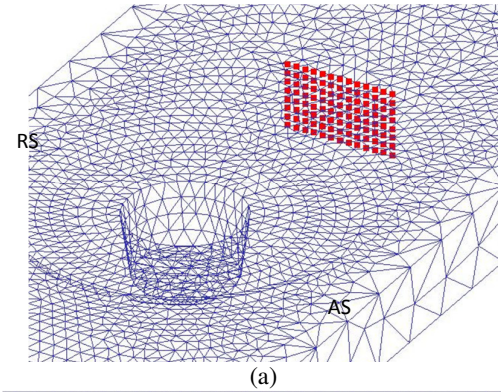

(a)

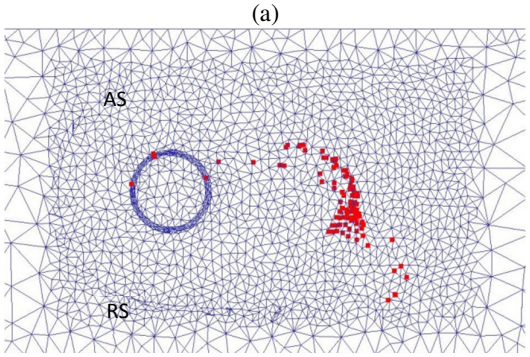

(b)

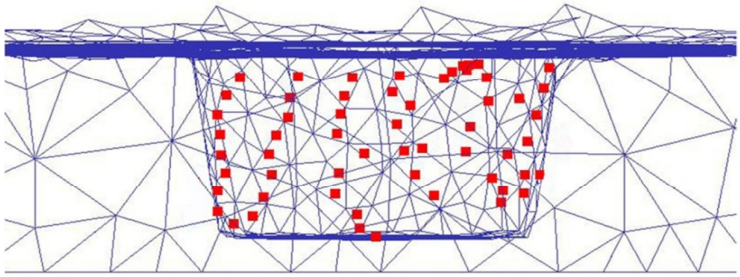

(c)

Fig12. (a) Initial position of points in front of tool which were picked for specification of overall material flow pattern, (b) and (c) final position of points.

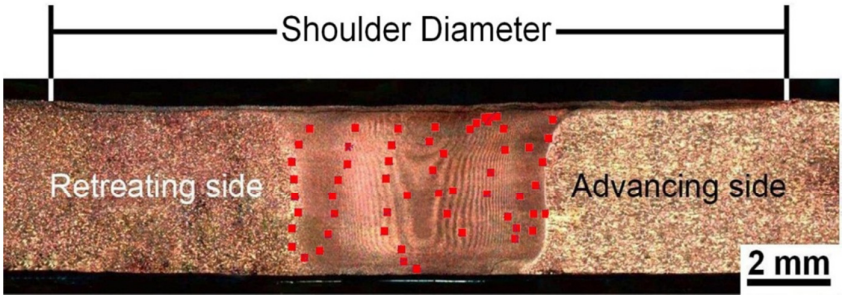

Fig13. Macro-image of SZ shape in friction stir welded copper plate [32]

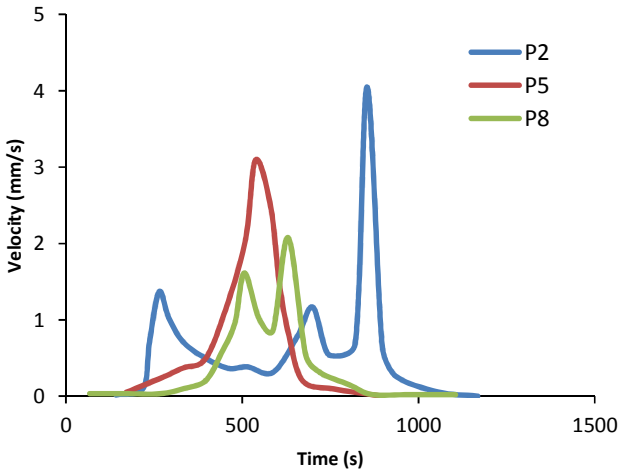

Fig14. Material velocity diagrams in the stir zone

9. . Material Flow Behavior

The material flow during FSW is complicated and directly influences the properties of FSWed work piece. It is of vital importance to understand the deformation process and basic physics of the material flow for optimal tool design. To visualize the material flow phenomenon, tracer particle set was defined along the welding line to track the material movement. Eight tracer particles, numbered 1 to 8, were used as illustrated in Figure 9. Points P1-P8 at their initial position located on the weld centre line with 0.5 mm increment in depth from the top surface.

Fig. 10 shows the material flow pattern on the centre of weld. Figure 10a-10d shows the position of those points as the time elapses. Fig. 11 shows final position of particles. Particle 1 starts to move around the pin with tool simultaneously, toward retreating side. At initial stages of process it rotates in a zone with diameter more than that of pin, due to high stress and strain rate and severe deformation in the region exactly below the tool shoulder. But as process proceeds, it moves finally to a zone with size equal to pin diameter, at the behind of tool pin. This behavior is almost the same for particle 2, which at first it is expelled from the region with size equal to pin diameter, but finally it resides in the that zone. It is interesting that these points reside finally in the behind of pin on the welding line, not behind advancing side, which reported in previous studies [26-27]. In fact these particles enters the shoulder/work piece interface, in a period of time, then pushed to inside of the zone with diameter equal to the pin diameter. The lower particles including No. 3 to No. 8 showed partially the same flow behavior however these particles always move near/inside of the zone with diameter equal that of pin. These points reside at the behind of pin, near joint line, and form

an asymmetric flow pattern with other points. The interesting point is point No. 6, which showed completely random flow manner. Also this point is the only point that resides at the advancing side. The complicated material flow behavior in FSW process is the reason for this case. Another important observation is that the height of particles does not change considerably. From mentioned observations, the material flow pattern can be characterized as following:

- Upper Zones: this zone is exactly below tool shoulder. Material flows along tool rotational path in a region with size larger than pin diameter. This severe material movement results from high stress and strain values in this region and remarkable material plastic deformation.

- Lower zones: this zone is around and inside of pin periphery, which material displacement is not as severe as the first zone, because stress and temperature are not adequate for material deformation in these regions. The whole material flow occurs inside the zone with size equal to pin diameter.

- Zone with random flow pattern: In this zone, material moves haphazardly. This region supports random metal flow pattern in FSW process.

A planar set of particles was selected for further investigation of material flow behavior, as shown in Figure 12a. Figures 12-b and 12-c show final position of points on from up and side views. As seen, they do not feed into neither AS nor RS, and this is in agreement with experimental macro photography of stirred zone in FSW of copper, which is shown in Figure 13 [32], where this case is completely different for Al alloys, in which, the stirred zone leans towards AS side [26-27]. Comparison of Figure 12c with Figure 13 indicates validity of presented numerical model. As seen, just a few points reside on the retreating side, far from the welding line.

10. . Material Flow Velocity

Material flow velocity is one of the key features of FSW process. Material flow velocity in the stirred zone was reported by Zhang et al. [11], and Buffa et al. [8], 0-17% and 5-8% of tool rotational speed, respectively. Some researchers considered material flow velocity equal to the tool rotational speed, in which, full sticking conditions is occurred. For three points on the welding line, (points No. 2, No. 5, and No. 8), material flow velocity was derived from simulations, as shown in Figure 14. These results show that in FSW of copper, material velocity is between 0-5 percent of tool velocity. The low values of velocity probably, contribute to high flow stress of copper, because more shear force is needed for material deformation and displacement. As seen, upper points experienced higher maximum velocity during process.

11. Conclusions

A 3D simulation based on lagrangian incremental formulation was developed for FSW of a copper alloy, in order to understand the material flow pattern using the point tracking. Additionally, temperature and effective plastic strain distributions, and material flow velocity were considered. Results show that:

Temperature distributions are not symmetric around welding line and maximum temperature occurs at the behind the tool pin.

Effective strain distribution around welding line is non-symmetric and its maximum value on the advancing side is more than that on the retreating side.

In FSW of copper, the stirred zone does not lean towards any sides of welding line completely, while this case is completely different for Al alloys.

Material velocity was 0-5% of tool rotational speed.

References:

[1]. Andersson, C.G., Andrews, R.E. Proceedings of the First International Symposium on Friction Stir Welding, Thousand Oaks, CA, USA, June, 1999.

[2]. Hautala, T., T. Tianien, T. David, S.A., DebRoy, T., Lippold, J.C., Smartt, H.B., J.M. Vitek, J.M. Proceedings of the Sixth International Conference on Trends inWelding Research, Pine Mountain, GA, ASM International, 2003.

[3]. Xue, P., Xiao, B.L., Zhang, Q., Ma, Z.Y. Achieving Friction Stir Welded Pure Copper Joints with Nearly Equal Strength to the Parent Metal via Additional Rapid Cooling. Scripta Materialia 2011, 64, 1051-1054.

[4]. Cederqvist, L., Sorensen, C.D., Reynolds, A.P., Öberg, T. Improved ProcessStability during Friction Stir Welding of 5 cm Thick Copper Canisters through ShoulderGeometry and Parameter Studies. Science and Technology in Welding andJoining 2009, 46(2), 178-184.

[5]. Guerdoux, S., Fourment, L. A 3D Numerical Simulation of Different Phases of Friction Stir Welding. Modeling and Simulation in Material Science and Engineering 2009, 17(7), 075001.

[6]. Xu, S., Deng, X., Reynolds, A.P., Seidel, T.U. Finite Element Simulation of Material Flow in

[7]. Friction Stir Welding. Science and Technology of Welding and Joining 2001, 6(3), 191-193.
[8]. Fourment, L., Guerdoux, S., Miles, M., Nelson, T. Proceedings of the 5th International Symposium on Friction Stir Welding, Metz, France, 2005.
[9]. Buffa, G., Hua, J., Shivpuri, R., Fratini, L. A Continuum based FEM model for Friction Stir Welding-Model Development. Material Science and Engineering A, 2006, 419, 389-396.
[10]. Schmidt, H., Hattel, J. A Local Model for the Thermomechanical Conditions in Friction Stir Welding. Modeling and Simulation in Material Science and Engineering 2005, 13(1), 77-93.
[11]. Schmidt, H., Hattel, J. Proceedings of the 6th International Symposium on Friction Stir Welding, Saint-Sauveur, Canada, 2006.
[12]. Zhang, H.W., Zhang, Z., Chen, J.T. 3D Modeling of Material Flow in Friction Stir Welding under Different Process Parameters. Journal of Materials Processing Technology, 2007, 183, 62-70.
[13]. Bendzsak, G.J., North, T.H., Smith, C.B. Proceedings of the Second International Symposium on Friction Stir Welding, Gothenburg, Sweden, June, 2000.
[14]. Shercliff, H.R., Colegrove, P.A. Modelling of Friction Stir Welding. Maney Publishing, 2002, 927-974.
[15]. Ulysse, P. Three-dimensional Modelling of the Friction Stir Welding Process. International Journal of Machine Tools and Manufacture, 2002, 42, 1549-1557.
[16]. Seidel, T.U., Reynolds, A.P. Two-dimensional Friction Stir Welding Process Model based on Fluid Mechanics. Science and Technology of Welding and Joining, 2003, 8(3), 175-183.
[17]. Colegrove, P.A., Shercliff, H.R. Two-dimensional CFD Modelling of Flow Round Profiled FSW Tooling. Science and Technology of Welding and Joining, 2004, 9(6), 483-492.
[18]. Colegrove, P.A., Shercliff, H.R. Development of Trivex Friction Stir Welding Tool Part 1: Two-dimensional Flow Modelling and Experimental Validation. Science and Technology of Welding and Joining, 2004, 9(4), 345-351.
[19]. Colegrove, P.A., Shercliff, H.R. Development of Trivex Friction Stir Welding Tool Part 2: Three-dimensional Flow Modelling. Science and Technology of Welding and Joining, 2004, 9(4), 352-361.
[20]. Colegrove, P.A., Shercliff, H.R. 3-Dimensional CFD Modelling of Flow Round a Threaded Friction Stir Welding Tool Profile. Journal of Materials Processing Technology, 2005, 169(2), 320-327.
[21]. Colegrove, P.A., Shercliff, H.R., Zettler, R. Model for Predicting Heat Generation and Temperature in Friction Stir Welding from the Material Properties. Science and Technology of Welding and Joining, 2007, 12(4), 284-297.
[22]. Nandan, R., Roy, G.G., DebRoy, T. Numerical Simulation of Three-dimensional Heat Transfer and Plastic Flow during Friction Stir Welding. Metallurgical and Materials Transactions A, 2006, 37, 1247-1259.
[23]. Bastier, A., Maitournam, M.H., Dang Van, K., Roger, F. Steady State Thermomechanical Modelling of Friction Stir Welding. Science and Technology of Welding and Joining, 2006, 11(3), 278-288.
[24]. Bastier, A., Maitournam, M.H., Roger, F., Dang Van, K. Modelling of the Residual State of Friction Stir Welded Plates. Journal of Materials Processing Technology, 2008, 200, 25-37.
[25]. Kim, D., Badarinarayan, H., Kim, J.H., Kim, C., Okamoto, K., Wagoner, R.H., et al. Numerical Simulation of Friction Stir Butt Welding Process for AA5083-H18 Sheets. European Journal of Mechanics A/Solids, 2010, 29, 204-215.
[26]. Buffa, G., Hua, J., Shivpuri, R., Fratini, L. A Continuum based FEM model for Friction Stir Welding-Model Development. Material Science and Engineering A, 2006, 419, 381-388.
[27]. Asadi, P., Mahdavinejad, R.A., Tutunchilar, S. Simulation and Experimental Investigation of FSP of AZ91 Magnesium Alloy. Materials Science and Engineering A, 2011, 528, 6469-6477.
[28]. Tutunchilar, S., Haghpanahi, M., Besharati, M.K., Asadi, P., Bahemmat, P. Simulation of Material Flow in Friction Stir Processing of a Cast Al-Si Alloy, Materials & Design, 2012, 40, 415-426.
[29]. Kobayashi, S., Oh, S., Altan, T. Metal Forming and the Finite Element Method, Oxford University Press, 1989.
[30]. Chang, C.I., Du, X.H., Huang, J.C. Scripta Materialia, 2007, 57, 209-212.
[31]. Prasad, Y.V.R.K., Rao, K.P. Processing Maps and Rate Controlling Mechanisms of Hot Deformation of Electrolytic Tough Pitch Copper in the Temperature range 300–950 °C. Materials Science and Engineering A, 2005, 391, 141-150.
[32]. Hwang, Y.M., Fan, P.L., Lin, C.H. Experimental Study on Friction Stir Welding of

Copper Metals. Journal of Materials Processing Technology, 2010, 210, 1667-1672.
[33]. Teimournezhad, J. Analytical Investigations on the Influence of the Welding Parameters in Friction Stir Butt Weld of Copper Plates, PhD Thesis, University of Tehran, 2010.